MULTISTATE ORNSTEIN-UHLENBECK SPACE USE MODEL REVEALS SEX-SPECIFIC PARTITIONING OF THE ENERGY LANDSCAPE IN A SOARING BIRD

By

Joseph M. Eisaguirre, B.A.

A Project Submitted in Partial Fulfillment of the Requirements

for the Degree of

Master of Science

in

Statistics

University of Alaska Fairbanks

December 2019

APPROVED:

Dr. Scott Goddard, Committee Chair
Dr. Ron Barry, Committee Member
Dr. Julie McIntyre, Committee Member
Dr. Margaret Short, Committee Member
Dr. Leah Berman, Chair
    Department of Mathematics & Statistics

Abstract

Understanding animals' home range dynamics is a frequent motivating question in movement ecology. Descriptive techniques are often applied, but these methods lack predictive ability and cannot capture effects of dynamic environmental patterns, such as weather and features of the energy landscape. Here, we develop a practical approach for statistical inference into the behavioral mechanisms underlying how habitat and the energy landscape shape animal home ranges. We validated this approach by conducting a simulation study, and applied it to a sample of 12 golden eagles *Aquila chrysaetos* tracked with satellite telemetry. We demonstrate that readily available software can be used to fit a multistate Ornstein-Uhlenbeck space use model to make hierarchical inference of habitat selection parameters and home range dynamics. Additionally, the underlying mathematical properties of the model allow straightforward computation of predicted space use distributions, permitting estimation of home range size and visualization of space use patterns under varying conditions. The application to golden eagles revealed effects of habitat variables that align with eagle biology. Further, we found that males and females partition their home ranges dynamically based on uplift. Specifically, changes in wind and the angle of the sun seemed to be drivers of differential space use between sexes, in particular during late breeding season when both are foraging across large parts of their home range to support nestling growth.

Keywords

---

[1]Eisaguirre, JM, TL Booms, CP Barger, CL McIntyre, GA Breed, S Goddard. 2019. Multistate Ornstein-Uhlenbeck space use models reveal sex-specific partitioning of the energy landscape in a territorial soaring bird. In prep for *Methods in Ecology and Evolution.*

Introduction

1 The home range concept has been a central idea in animal behavior for some time (Burt,

2 1943; Dunn and Gipson, 1977). To help understand an animal's home range—the area

3 in which an animal carries out its regular activities of foraging and reproducing (Burt,

4 1943)—researchers have applied techniques ranging from simple and purely descriptive,

5 including minimum convex polygons and kernel density estimators, to complex mecha-

6 nistic models, such as advection-diffusion equations (Moorcroft and Lewis, 2006; Hooten

7 et al., 2017). Within this range fall methods framed as resource selection functions

8 (RSF; Manly et al., 2002) and related techniques, such as step selection functions (SSFs;

9 Fortin et al., 2005). The RSF and SSF frameworks separate the probability of an animal

10 occurring somewhere on a landscape into two parts: movement and resource selection

11 (Moorcroft and Barnett, 2008). Together, movement and resource weighting functions

12 can give rise to diverse animal space use patterns (Potts et al., 2014b).

13 One proposed conceptual description of animal home ranges aligns with the "elastic

14 disc hypothesis," which describes animal space use as the degree to which boundaries of

15 animal territories are compressible, shaped by the territorial aggression of neighboring

16 conspecifics (Huxley, 1934). This processes is analogous to the way an elastic disc can be

17 molded by extrinsic stressors, and the analogy forms a general conceptual foundation de-

18 scribing the formation and dynamics of animal home ranges (Getty, 1981). For example,

19 consider an animal that requires a certain amount of suitable habitat. Given no extrinsic

20 forces, that animal might spend much of its time within a smaller core area, venturing

21 out equally in all directions to acquire resources. This would give rise to a circular or

22 disc-shaped home range, and would be especially true for an animal that has a "central

23 place" such as a nest of a den that requires tending. In contrast, if the animal resides

24 near the boundary of suitable habitat, its home range must stretch along that boundary,

25 as the amount of suitable habitat that the animal requires remains constant, so the shape

26 of the home range will conform to habitat constraints.

27 Many approaches to quantifying animal home ranges describe animal space use as

28 static, either because the descriptive method is not capable of dynamic description or

home ranges are actually assumed to be static. However, animal movement is usually much more fluid, driven by suites of intrinsic and extrinsic forces (Nathan et al., 2008). Dynamic energy landscapes are a conceptual framework that incorporates such fluidity in how an animal's movement can be shaped by its energetic demands interacting with landscape features (Shepard et al., 2013). Such dynamic changes in the landscape can shape space use patterns in a number of ways (Morales and Ellner, 2002; Schooley and Wiens, 2004; Prokopenko et al., 2016). For animals that can take advantage of dynamically available energy subsidies from moving fluids to offset energy expenditure, such as soaring birds using uplift or aquatic animals taking advantage of water flow, these features will shape dynamic space use patterns and emergent home range properties (Shepard et al., 2013). In these situations, the elastic disc will constantly vary, changing shape just as continuously as changes in the weather.

RSFs and SSFs are widely used and generally robust quantitative assessments of animal space use and home range dynamics, and they have seen continuous improvement since their respective introductions. Some of these adaptations have worked to address such dynamic home range processes (reviewed by Hooten et al., 2017) but few of these developments are particularly useful or flexible in analyses of the dynamic properties of space use patterns. Getty (1981) presented an early RSF adaptation inspired by the elastic disc hypothesis. Another early model has also been considered in understanding animal home ranges—the Ornstein-Uhlenbeck (OU) proccess (Dunn and Gipson, 1977)— and can align with the elastic disc hypothesis. As we show herein, when linked to an RSF framework (Johnson et al., 2008), the OU process can be useful for drawing inferences about the underlying mechanisms that give rise to dynamic space use patterns and home range formation.

Here, we develop a practical modelling approach for inferring the mechanisms of home range dynamics and how habitat and the energy landscape interact with behavior to shape animal home ranges. This approach was then validated using a simulation study to ensure it provided robust, unbiased inference, and we finally applied the approach to analyze the home range behavior and space use of territorial golden eagles *Aquila chrysaetos*. Specif-

4

58 ically, we fit models to estimate how male and female territorial eagles partitioned space
59 based on different habitats or dynamic features of the landscape, particularly thermal
60 and orographic uplift. Our method is an adaptation of a previous method and allows
61 relatively straightforward hierarchical inference of resource selection parameters across
62 several individuals within an OU home range model.

Ornstein-Uhlenbeck home range model

An OU process over two-dimensional space is continuous-time, mean-reverting, and can help us study home range behavior of animals that tend a central place (e.g., a nest; Dunn and Gipson, 1977; Blackwell, 1997; Breed et al., 2017). Assuming independence in the two spatial dimensions simplifies the model and aligns better with central place behavior, as movement is equally likely in all directions around the central point. Such an OU process can be presented as the following stochastic differential equation (SDE):

$$d\mathbf{x}_t = -\boldsymbol{\omega} dt(\mathbf{x}_t - \boldsymbol{\mu}) + \sigma d\mathbf{W}_t, \tag{1}$$

where $\mathbf{x}_t$ is a coordinate vector of the location of the animal at time t, $\boldsymbol{\omega} = \omega \mathbf{I}_2$ with ω describing the strength of the animal's tendency to move toward the central point $\boldsymbol{\mu}$, $\sigma > 0$, and $\mathbf{W}_t$ is Brownian motion. The solution of this SDE takes the form:

$$\mathbf{x}_t = \boldsymbol{\mu} + e^{-\boldsymbol{\omega} t}(\mathbf{x}_0 - \boldsymbol{\mu}) + \sigma \int_0^t e^{-\boldsymbol{\omega}(t-s)} d\mathbf{W}_s. \tag{2}$$

While this solution conveniently gives the position of the animal at any time t, we typically observe animal movement by recording series of discrete locations by, for example, using telemetry. This invokes the position likelihood of the OU process:

$$\mathbf{x}_t | \mathbf{x}_{t-\Delta t} \sim \mathcal{N}\left(\boldsymbol{\mu} + e^{-\boldsymbol{\omega}\Delta t}(\mathbf{x}_{t-\Delta t} - \boldsymbol{\mu}), \ \boldsymbol{\Sigma} - e^{-\boldsymbol{\omega}\Delta t}\boldsymbol{\Sigma}e^{-\boldsymbol{\omega}'\Delta t}\right), \tag{3}$$

64 where $\boldsymbol{\Sigma} = \sigma^2 \mathbf{I}_2$ and $'$ denotes the transpose. This discretized formulation can be de-
65 scribed as a biased random walk (BRW) with a bias toward $\boldsymbol{\mu}$. Notably, it reaches a long

5

term steady state $\mathcal{N}(\boldsymbol{\mu}, \boldsymbol{\Sigma})$ due to the rapidly decaying effect of conditioning on $\mathbf{x}_t$ as Δt increases (Blackwell, 1997).

Assuming independence in the two spatial dimensions helps wed the OU process to the elastic disc hypothesis (Huxley, 1934; Getty, 1981), similar to the circular normal distribution used by Getty (1981). A chosen contour of $\mathcal{N}(\boldsymbol{\mu}, \boldsymbol{\Sigma})$ can be a circular approximation of an animal's home range. Further, the highest probability density of $\mathcal{N}(\boldsymbol{\mu}, \boldsymbol{\Sigma})$ is centered on $\boldsymbol{\mu}$, consistent with central place behavior. Note that using equation (3) takes into account serial correlation, which is inherent to an animal's movement, ensuring an unbiased estimate of $\boldsymbol{\Sigma}$. Additionally, the continuous-time nature of the process makes it applicable under any temporal resolution of data and any irregularities in that data.

The disc may be modified by various extrinsic factors (Getty, 1981), which can be built into the OU process under the RSF framework (Johnson et al., 2008). The general form of this framework describes the probability density f_u of an animal's location over some landscape (and respective coordinate system) $\mathbf{z}$ containing a suite of habitat types and resources as the product of a density explaining what is available to the animal f_a and a weighting function ψ:

$$f_u(\mathbf{z}) = K^{-1}\psi(\mathbf{z})f_a(\mathbf{z}), \tag{4}$$

where K is a normalizing constant. When f_a takes the form of an OU process and $\psi(\mathbf{z}(\mathbf{x}_t)) = \exp[\mathbf{z}(\mathbf{x}_t)'\boldsymbol{\beta}]$, where the function $\mathbf{z}(\mathbf{x}_t)$ returns a vector of habitat values and/or resources associated with a location $\mathbf{x}_t$ that lies in $\mathbf{z}$ and $\boldsymbol{\beta}$ weights those resources based on the animal's preferences, the conditional probability density of the location of the animal can be written (Johnson et al., 2008) as

$$f_u(\mathbf{z}|\mathbf{x}_{t-\Delta t}) = K^{-1}\exp[\mathbf{z}(\mathbf{x}_t)'\boldsymbol{\beta} - (\mathbf{x}_t - \boldsymbol{\mu}_t)'\boldsymbol{\Sigma}_t^{-1}(\mathbf{x}_t - \boldsymbol{\mu}_t)/2], \tag{5}$$

where $\boldsymbol{\mu}_t = \boldsymbol{\mu} + e^{-\omega\Delta t}(\mathbf{x}_{t-\Delta t} - \boldsymbol{\mu})$ and $\boldsymbol{\Sigma}_t = \boldsymbol{\Sigma} - e^{-\omega\Delta t}\boldsymbol{\Sigma}e^{-\omega'\Delta t}$.

The likelihood function takes the form:

$$L(\boldsymbol{\beta}, \boldsymbol{\omega}, \boldsymbol{\Sigma}, \boldsymbol{\mu}) = \prod_{t=1}^{T} \frac{\exp[\mathbf{z}(\mathbf{x}_t)'\boldsymbol{\beta} - (\mathbf{x}_t - \boldsymbol{\mu}_t)'\boldsymbol{\Sigma}_t^{-1}(\mathbf{x}_t - \boldsymbol{\mu}_t)/2]}{\int_Z \exp[\mathbf{z}(\mathbf{x})'\boldsymbol{\beta} - (\mathbf{x} - \boldsymbol{\mu}_t)'\boldsymbol{\Sigma}_t^{-1}(\mathbf{x} - \boldsymbol{\mu}_t)/2 \, d\mathbf{x}}, \tag{6}$$

6

77 where $\boldsymbol{\mu}_t$ and $\boldsymbol{\Sigma}_t$ contain the OU process parameters, as defined above for equation (5)

78 (Johnson et al., 2008). Evaluating the integral in the denominator is usually problematic

79 but often avoided in estimating $\boldsymbol{\beta}$ with more conventional RSF models by implement-

80 ing an use-availability design that compares resources at 'available' locations to 'used'

81 locations with logistic regression (Lele and Keim, 2006; Hooten et al., 2017). We note

82 that equation (6) resembles a more conventional RSF likelihood with an offset term—the

83 anisotropic distance between $\mathbf{x}_t$ and $\mathbf{x}_{t-\Delta t}$ (Johnson et al., 2008). We consequently posit

84 that if the OU process parameters were estimated first, then were used to construct the

85 necessary covariate, $\boldsymbol{\beta}$ could then be estimated in a second step with regression, which is

86 similar to constructing covariates for estimating $\boldsymbol{\beta}$ with Poisson regression (Johnson et al.,

87 2013) and conditional logistic regression (Forester et al., 2009). Although a sacrifice in

88 statistical elegance, this saves considerable model complexity and estimation challenge,

89 especially when hierarchical inference of $\boldsymbol{\beta}$ across several individuals is a primary goal. In

90 doing so, we use point estimators to computing the covariate, which unfortunately also

91 sacrifices ensured unbiased uncertainty around $\boldsymbol{\beta}$. However, resource selection methods

92 that use fitted parametric distributions to characterize availability often similarly disre-

93 gard the uncertainty around the estimated parameters of those parametric distributions

94 (e.g.; Avgar et al., 2016). The possible effects of discounting that uncertainty on inference

95 likely warrant further study, however.

96   A primary advantage of the OU model within this framework is that it explicitly

97 weights locations closer to the central point $\boldsymbol{\mu}$ more heavily. If it did not, space use

98 in that area would be attributed solely to habitat or resources there, which could bias

99 $\hat{\boldsymbol{\beta}}$. Another advantage of this OU model is that it can be used to build a home range

100 estimate from a set of hypothesized mechanisms, such as different, possibly interacting,

101 and/or dynamic habitat variables. Given that ψ is assumed stationary and as Δt gets

102 large f_a approaches $\mathcal{N}(\boldsymbol{\mu}, \boldsymbol{\Sigma})$,

$$\lim_{\Delta t \to \infty} f_u(\mathbf{z}|\mathbf{x}_{t-\Delta t}) = K^{-1}\exp[\mathbf{z}(\mathbf{x}_t)'\boldsymbol{\beta}]\exp[-(\mathbf{x}_t - \boldsymbol{\mu})'\boldsymbol{\Sigma}^{-1}(\mathbf{x}_t - \boldsymbol{\mu})/2], \qquad (7)$$

103 which is simply the normalized product of a multivariate normal kernel (i.e. our elastic

disc) and the habitat weighting function. We are thus left with a disc—a habitat independent central place only (circular) home range estimator $\mathcal{N}(\boldsymbol{\mu}, \boldsymbol{\Sigma})$—and a weighting function ψ that shapes the disc. The product of these provides the stationary estimate of f_u, a contour of which is conceptually the elastic disc molded by the habitat (Fig. 1). It is worth noting here that equation (7) is key because if this property, which is owed to the OU process, were not true, then a computationally intensive simulation procedure or numerical investigation of the master equation would be required to construct a home range or space use estimate (Moorcroft and Lewis, 2006; Barnett and Moorcroft, 2008; Potts et al., 2012, 2014a,b,c; Potts and Lewis, 2014; Signer et al., 2019), rather than simply taking the product of two densities.

Simulation study

Methods To ensure that estimation of the OU process and resource selection parameter estimates were unbiased and informative, we implemented a simulation validation generally following the approaches of Forester et al. (2009) and Johnson et al. (2008). The simulation began with the creation of three artificial landscapes containing a continuous resource variable. Using R and the package `RandomFields` (R Core Team, 2018; Schlather et al., 2019), landscapes were generated on a 2000×2000 grid using a Gaussian random field (GRF) with an exponential covariance function. The scale parameter was set at 10, 50, or 100, prescribing each landscape a different level of spatial autocorrelation. We simulated 100 tracks, each 100 move steps in length, for each landscape and each of six parameter combinations ($\beta = 0, 1$, or 2 and $\omega = 1$ or 2) for a total of 18 landscape/parameter scenarios. σ^2 was fixed at 100^2 and $\boldsymbol{\mu}$ at $(1000, 1000)$. For each simulated track, we fit the OU model, assuming the central point $\boldsymbol{\mu}$ known, generated available points, computed the necessary covariate from the estimated OU parameters, and then attempted to estimate β with an use-availability design using logistic regression.

Estimation was performed in a Bayesian framework using Stan with R (Stan Development Team, 2016, 2018; R Core Team, 2018), sampling five available points for each

used point from the marginal posterior predictive distributions of each $\mathbf{x}_t$ (Hooten et al., 2014, 2017; Eisaguirre et al., 2019). We used three chains of 15,000 iterations, including 5,000 for warm-up, and retained 1,000 samples for inference in fitting the OU movement model, and we used four chains of 5,000 iterations, including 3,000 for warmup, and retained 2,000 samples for inference in estimating the selection parameter β. Weakly informative (truncated) normal priors were placed on the OU parameters, centered away from the true values, and a weakly informative normal prior on β, centered on zero. (See Appendix 2 for code containing details about the priors.) The covariate that accounts for the OU movement process in estimating β (equation 5) was computed for each used and available point with the posterior means from estimating the OU process. β was then estimated with an use-availability design and Bayesian logistic regression. For each parameter combination, we summarized the relative biases of the posterior means and the proportion of tracks for which the 95% credible interval overlapped the true value for β, ω, and σ^2.

Simulation Results The proportions of 95% credible interval coverage were > 0.80 for nearly all cases in estimates of β (three were > 0.70) and generally high for σ^2 and ω as well (Figs. S1 & S2). Thus, simulations generally found the two-step approach provided estimates of resource selection parameters β with no or minimal bias (Fig. 2). Other use-availability designs have also been found to yield unbiased estimates of resource selection parameters (Lele and Keim, 2006; Forester et al., 2009; Avgar et al., 2016). Estimating the movement parameters ω and σ^2 yielded slightly more bias but generally similar to bias resulting from maximizing the full conditional likelihood, as found in the simulation study of Johnson et al. (2008).

Separating within home range movement and selection parameters remains inherently difficult for any estimation method. For example, probability of use could be high in certain spatial locations due to (1) the presence of a home range center (e.g., nest or den) or (2) the presence of a highly favorable habitat feature. The OU home range model partially accounts for these confounding reasons for use of some areas within home ranges, but consistent with the findings of Johnson et al. (2008), identifiability of the two

160 movement and selection parameters/processes remains a serious modelling challenge.

Application

Model system

163 Golden eagles are a long-lived, territorial raptor that reach sexual maturity entering their
164 third breeding season (Kochert et al., 2002; Watson, 2010). They most commonly nest on
165 cliffs, or less commonly large trees, and are generally central place foragers (Kochert et al.,
166 2002; Watson, 2010). Eagles with established territories where a nest is a central place
167 surrounded by uniformly average landscape should be expected to range and and use space
168 in a circular pattern around the nest. Because real landscapes are not uniform, an eagle's
169 realized space use would then be shaped by the habitat surrounding that central point.
170 Primary prey of Alaskan golden eagles are snowshoe hare *Lepus americanus*, ptarmigan
171 *Lagopus* spp., and Arctic ground squirrel *Urocitellus parryii* (McIntyre and Adams, 1999;
172 McIntyre and Schmidt, 2012; Herzog et al., 2019).

173   When a pair of eagles initiate a nesting attempt, the male does the majority of the
174 provisioning, while the female tends the nest and does most of the incubating and brood-
175 ing of eggs/nestlings. When nestlings mature to the point that they can thermoregulate
176 (or when a nest fails), the adult female no longer needs to incubate or shade them as
177 regularly, so she is free to move about the territory and aid provisioning (Watson, 2010).
178 We expect that this event should be commensurate with an abrupt change in space use,
179 because nest tending requirements suddenly become less restrictive. This might allow
180 space use to change so that the male and female of the breeding pair partition space to
181 minimize overlap in foraging areas and/or territory defense efforts. It is also possible
182 that this might occur dynamically throughout the season and/or day, regardless of nest
183 tending duties.

184   Another key characteristic of golden eagles that would be expected to strongly in-
185 fluence how they use space is their flight mechanics—they are a soaring bird capable
186 of capturing dynamic air currents to decrease or completely offset the energetic costs of

10

flight (Katzner et al., 2012; Watson, 2010). Consequently, their space use patterns, and possibly partitioning of space among individuals, will be shaped dynamically by weather variables. Two common forms of such flight subsidies are thermal uplift, caused by the sun heating the surface of the earth and causing air to rise, and orographic uplift, caused by wind blowing up slope.

Extension to multiple home range cores

Because habitat and weather features are non-uniform around nest sites/central places, eagles (and other animals) can establish multiple core areas within their larger home range. Thus real home ranges are not a single circular distribution in a homogeneous landscape, but multiple approximately round cores shaped by the non-uniform distribution of food and energy subsidies.

An OU home range model can be extended to allow for multiple core areas, and each core can be allowed to have a unique set of movement patterns, within an animal's broader home range (Johnson et al., 2008; Breed et al., 2017). The simplest method to accomplish this is estimating transitions among K cores as a Markov process, with a $K \times K$ transition matrix $\boldsymbol{\Gamma}$ describing the probability of the animal moving from one core to another (or remaining in the currently occupied core) during the time interval t to $t + 1$ (Breed et al., 2017). Note that to ensure the Markov assumptions hold, fixed and regular time intervals are required, which is common in most (but not all) types of telemetry data. We can also estimate the relationships between transition probabilities and habitat conditions or other covariates in a manner similar to multinomial logistic regression. As these covariates can be temporally dynamic, we may denote our transition matrix as $\boldsymbol{\Gamma}_t = (\gamma_{ij,t})$. Employing the multinomial logit link, we can write the conditional probability that the animal is in the jth core at time $t + 1$ given that it came from the ith core:

$$P(k_{t+1} = j | k_t = i) = \gamma_{ij,t} = \frac{\exp(\gamma_{ij,t}^*)}{\sum_{k=1}^{K} \exp(\gamma_{ik,t}^*)} \tag{8}$$

where $\gamma_{ij,t}^* = \mathbf{S}_{ij,t}'\boldsymbol{\alpha}_{ij}$. $\mathbf{S}_{ij,t}$ is the vector of covariates associated with the core $k_t = i$ at time t, and the vector $\boldsymbol{\alpha}_{ij}$ weights those covariates by their effect on $\gamma_{ij,t}$. We could thus calculate $\boldsymbol{\Gamma}_t$ for a set of core- and time-specific covariates. This is similar to modeling behavioral state transitions with a conventional hidden Markov Model for animal movement data (*sensu* Michelot et al., 2016), but the 'states' here are home range cores, each having a respective set of movement parameters (Breed et al., 2017).

Unsupervised estimation of the state transitions, which in Stan required marginalizing the latent discrete process, proved computationally impractical. We thus followed Breed et al. (2017) and implemented a k-means clustering algorithm to identify each home range core center $\boldsymbol{\mu}_k$ and the core transitions a priori. We then proceeded with supervised estimation of $\boldsymbol{\Gamma}_t$ and assuming each $\boldsymbol{\mu}_k$ known.

Telemetry data

We captured golden eagles with a remote-fired net launcher placed over carrion bait near Gunsight Mountain, Alaska (61.67°N 147.35°W). Captures occurred during spring migration, mid-March to mid-April 2014-2016. Adult and sub-adult eagles were equipped with 45-g back pack solar-powered Argos/GPS platform transmitter terminals (PTTs; Microwave Telemetry, Inc., Columbia, MD, USA). Eagles were sexed molecularly and aged by plumage.

PTTs were programmed to record GPS locations on duty cycles, ranging from 8-14 fixes per day during the breeding season, depending on year of deployment. In 2014, PTTs were set to record 13 locations at one-hour intervals centered around solar noon plus a location at midnight local time. 2015 PTTs were programmed to record eight locations with one-hour intervals centered around solar noon very early and late in the season and 10 locations for most of the season. In 2016, we revised our programming approach so that PTTs took 12 fixes with a fixed 2-hr time interval. Fifteen PTTs were deployed in 2014, 23 in 2015, and 15 in 2016.

Covariates

Selection covariates We used the Alaska Center for Conservation Science Alaska Vegetation and Wetland Composite (AKVWC; 30-m resolution) data for characterizing habitat type. We collapsed the numerous habitat types in the dataset into eight for this analysis. These were shrub, open (e.g., meadows and open tundra), bare, forest, wet (e.g., marsh), water, ice (i.e. perennial snow and ice), and human. See Appendix for details.

Elevation data were gathered using the Mapzen Terrain Service with the `elevatr` package (Hollister and Shah, 2018). We specified the 'zoom' variable such that the resolution closely matched that of the habitat data. We included elevation and slope ($slope \in [0, \pi/2]$ radians) as predictors in the model.

We used a state-wide data set of snow-off date (date of which an area became snow free) to derive a dynamic binary indicator variable of whether or not grid cells were free of snow (Macander et al., 2015). While one might expect some confounding between the (perennial) snow and ice habitat variable and this snow indicator, it would be limited due to few glaciated and perennial snow-covered areas frequented by eagles sampled.

The remaining variables included in the model were related to orographic and thermal uplift and were derived from the National elevation data and Center for Environmental Predictions (NCEP) North American Regional Reanalysis (NARR) data. Angle of incidence (aoi) was included for the effect of orographic uplift on eagle space use. It is the deviation of the relative wind from the aspect of a slope and was computed such that $aoi \in [0, \pi]$ (Murgatroyd et al., 2018); $\pi/2$ corresponds to a wind orthogonal to a slope's aspect, and π to a wind perfectly parallel blowing up slope. Wind direction was computed trigonometrically from the meridional and zonal wind components estimated by the NCEP NARR 10 m above the surface.

The effect of thermal uplift was included with a hill shade variable. Hill shade was computed following Murgatroyd et al. (2018), such that $hs \in [0, 1]$, where $hs = 1$ is direct sun (most thermal uplift) and $hs = 0$ no sun (no thermal uplift). We gathered the required location-, date-, and time-specific azimuth and zenith of the sun using the package `maptools` (Bivand and Lewin-Koh, 2016).

13

Core switching covariates We also included wind variables as covariates in the core transition process. We expected that certain wind directions and/or magnitudes might make certain home range cores more or less favorable. So, the cosine and sine of wind direction were included in addition to wind magnitude as covariates in equation (8). As above, these were computed trigonometrically from the NCEP NARR data specific to each home range core.

Inference

Due to the Markov assumption, we used only the tags deployed in 2016 programmed for a uniform fix rate, and given our primary goal was to illustrate this approach, here, we used only data for territorial eagles in 2016. This included six males and six females, all aged to their fifth year or older. None of these eagles were members of the same pair. Aerial surveys flown in June 2016 revealed that four of the eagles had young (at the time of the survey), and, with the exception of one nest site that was not surveyed, the others showed signs of reproductive attempts.

The model was fit as described above for simulations. However, we used three chains of 3,000 iterations, including 2,000 for warmup, retaining 3,000 samples for inference in estimating the OU process parameters and four chains of 2,000, including 1,000 for warmup, retaining 2,000 samples for inference in estimating the selection parameters. Weakly informative normal priors were placed on α_{ij}. Convergence of the posterior was checked with trace plots and Gelman diagnostics (Stan Development Team, 2018). Stan and R code for fitting the OU process and sampling from the conditional posterior predictive distributions are provided in Appendix 2.

As our primary interest was differences between male and female eagles in early and late breeding season, we wanted parameter estimates specific to each sex and to early and late breeding season. To keep computing time more reasonable, we fit the model separately for these periods as well as for each sex, as opposed to using indicator variables in a single model fit. The OU parameters were estimated separately for each individual, but the selection coefficients β were estimated hierarchically across individuals in the

295 regression model. Aerial observations of the nests of the tagged eagles indicated that

296 20 June was on average the approximate date when chicks should have been of age to

297 thermoregulate, so that is the date we used to partition the data between early and late

298 breeding season.

299 Space use distributions were computed according to equation (7). The probability

300 density predicted for each home range core was weighted by the number of eagle locations

301 in that core prior to computing the 95% volume contour of the space use distributions,

302 which we used to estimate home range boundaries. 95% is fairly consistent across more

303 descriptive home range estimation techniques (Hooten et al., 2017).

Results

Movement parameters

306 Because individuals had differing numbers of home range cores, we summarize here only

307 the OU movement parameters from each individual's most heavily used core. We found

308 some variation in OU parameters between sexes and periods of the breeding season (early

309 vs. late) for territorial golden eagles (Fig. 3 & 4). These patterns provide some evidence

310 for an increase in home range core size, indicated by larger or more variable $\hat{\sigma}$ (Fig. 3)

311 and increase in home range structure, based on an increase in number of home range

312 cores (Fig. 4) for females. There was also a slight decrease in the central tendency $\hat{\omega}$

313 within the most used core (Fig. 3). Finally, for some eagles, there was evidence that

314 wind affected switching between core areas for individuals with multi-core home ranges

315 (Fig. 3).

Habitat selection

317 We present the effects of the most relevant habitat types in figure 5 and provided figure

318 S4 with all effects in Appendix 1. Both male and female eagles weakly selected against

319 forested areas during early breeding season, and females seemed to select against shrub

320 and open habitats early, relative to bare areas (Fig. 5). Overall, males and females

321 selected for similar terrain, though there was some evidence that females selected for

15

322 slightly steeper slopes (Fig. S3).

Energy landscape

324 In the early breeding season, before chick thermoregulation or nest failure allow more
325 movement away from the nest, males and females appears to select energy landscape
326 features similarly (Fig. 6, 7, & 8).

327 During late breeding season, male and female eagles appeared to partition the land-
328 scape dynamically based on components of the energy landscape (Fig. 6, 7, & 8). Males
329 tended to use areas with more orographic uplift (i.e. higher angle of incidence; Fig. 6),
330 while females used more thermal uplift (i.e. greater hill shade; Fig. 6). This pattern
331 most likely resulted from males and females selecting dynamic energy subsidy features
332 differently (Fig. 7). Further, females showed essentially no selection for or against angle
333 of incidence during late breeding season (Fig. 6 & 7). The posterior probability that
334 females selected more strongly for hill shade than males was 0.06, and the posterior prob-
335 ability that males selected more strongly for higher angle of incidence than females was
336 0.18 (Fig. 7). We computed these as the number of female (or male) posterior samples
337 that were greater than the male (or female) posterior mean divided by the total number
338 of samples.

Discussion

340 Our most notable finding from applying the OU space use model to territorial golden
341 eagles was that male and female eagles seem to partition the energy landscape during late
342 breeding season when both sexes would be using the home range and possibly provisioning
343 young (Fig. 6 & 7). Two possible explanations for this dynamic partitioning of space
344 could be (1) a means for each sex to avoid overlap in foraging and/or territory defense
345 efforts and/or (2) an emergent pattern resulting from sexual size dimorphism.

346 Avian taxa vary in morphology to utilize different types of flight (e.g., flapping or
347 soaring) but there are also morphological differences within soaring taxa, such that cer-
348 tain species are better adapted for different types of soaring, including dynamic, slope,

and thermal (Gill, 2007). Between sexes of species, though, we also find differences. For example, the females of many raptors, including golden eagle, exhibit higher wing loading (wing area per body mass) than males (Lish et al., 2016). Lighter wing loading could allow male eagles to capitalize on even slight bits of uplift generated orographically with more energetic efficiency than females. Thermal uplift is also generally a more efficient flight subsidy than orographic uplift (Duerr et al., 2012), so, given their higher wing loading, it might be energetically advantageous for females to use primarily thermal soaring. Further, Murgatroyd et al. (2018) found among-territory variation in how different dynamic variables predict Verreaux's eagles' soaring modes; however, they did not report the sexes of the eagles tagged. Given our results, it is possible that some of that variation could have also been due to sex-specific use of the energy landscape.

Orographic uplift is typically available at only relatively low heights above Earth's surface, whereas thermals can travel much higher into the atmospheric boundary layer. The altitude of eagles using these different types of uplift follows suit (Katzner et al., 2015). Given selection for differing types of uplift, we would thus expect male and female eagles might also partition their home ranges vertically as well. Maintaining good visibility with the surface is required for successful foraging, so partitioning thermal and orographic uplift could indicate different behavioral budgets or hunting strategies. Males could more frequently forage, while the larger females might spend more time thermal soaring at higher altitudes poised to defend the territory against conspecific intruders. In previous work, females have been reported to be more active in nest and territory defense than males (Bahat, 1989), likely especially in late breeding season when they are more free from tending young, which corresponds to the period when we found partitioning of the energy landscape (Fig. 6 & 7). It is important recognize that thermal and orograpahic uplift vary over space following changes in wind and the angle of the sun. Consequently, males and females may partition space and activities temporally though the day, as females may await better thermal soaring conditions during the day before beginning extensive movements around the home range. In contrast, wind can generate orographic uplift throughout the day.

17

While our findings relating to the energy landscape were most notable, we also found some differences in habitat and terrain use, which are consistent with sex-specific roles during the breeding season. Females used and selected steeper slopes than males, consistent with nesting behavior and perching near the nest (Collopy and Edwards, 1989; Kochert et al., 2002; Watson, 2010). Not surprisingly, females used less steep slopes during late breeding season, compared to early, consistent with behavior in the later nestling stages of breeding (Watson, 2010). Also, males, who do most of the provisioning even late into the breeding season (Collopy and Edwards, 1989; Watson, 2010), selected more strongly for shrub and open habitats (Fig. 5), which would likely be used for hunting. During late breeding season, females' selection for shrub habitats approached that of bare areas, likely following an increased role in provisioning. We also saw changes in movement patterns and home range structure consistent with this as well (Fig. 3 & 4). Additionally, females selected most strongly for bare areas, which could be related to the energy landscape, as bare ground would gather the most solar radiation to generate thermal uplift.

There were few general patterns in how eagles transitioned among home range cores following changes in wind (Fig. 3), but we did successfully estimate the Markovian transition process. This was similar to Breed et al. (2017), but we modeled all transition probabilities with covariates. In fact, we found that estimation of this multistate OU model was relatively easy with Stan, as convergence to the posterior was rapid. One possible biological pattern that we found was that females tended to avoid departing their most used use core area in windier conditions during early breeding season (Fig. 3). During windier, colder conditions, female golden eagles will spend additional time incubating and brooding (Collopy, 1984).

Finally, predictions of home range size from the fitted model were similar to home range sizes estimated for golden eagles using descriptive techniques (Fig. 9; Watson, 2010; Watson et al., 2014; Moss et al., 2014; Braham et al., 2015). While there were some notable large home ranges predicted (Fig. 9), these were from individuals that had failed at breeding, some of which made some larger scale movements away from their

apparent territory. So, home ranges estimated from the fitted OU space use model are likely reasonably representative of eagle space use patterns. Although our simulation study suggested that $\hat{\sigma}$, on which our predictions of home range size strongly depend, can be biased, that would be expected when β (and spatial autocorrelation) is high, but our results in this application suggest β is relatively low for the eagles sampled (Fig. 5 & 7). Nonetheless, our estimates of the OU parameters and predictions of home range size should be interpreted cautiously.

Conclusions

We showed that estimating a fairly complex mechanistic space use model is relatively flexible and can be done by leveraging readily available software. While the model works most naturally with central place animals, the ability to incorporate multiple home range cores, and considering the range of movement and space use patterns that can be captured with the OU parameters, make it quite broadly applicable. Further, the simplicity in computing estimates of space use distributions and home range boundaries—the product of two steady-state distributions—is an additional attribute (Fig. 1 & 9).

In applying the model to a sample of golden eagles, we were able to obtain hierarchical inference of habitat selection parameters quite easily. In doing so, although our sample consisted of only 12 individuals, we provided some evidence of sex-specific partitioning of the energy landscape within home ranges, in addition to some other movement and habitat selection patterns consistent with eagle biology. Sex-specific patterns in utilizing the energy landscape, perhaps across a breadth taxa beyond soaring birds, is certainly worth further study.

Acknowledgements

19

through the federal State Wildlife Grant Program. JME was supported by the Calvin J. Lensink Fund during part of the project.

Data accessibility

All movement data used for this manuscript are managed in the online repository Movebank (`https://www.movebank.org/`; IDs 17680093 and 19389828). The data contain information considered confidential and sensitive by the State of Alaska (State Statute 16.05.815(d)), but they could be made available for research at the discretion of the Alaska Department of Fish & Game.

References

Avgar T, Potts JR, Lewis MA, Boyce MS. 2016. Integrated step selection analysis: Bridging the gap between resource selection and animal movement. *Methods in Ecology and Evolution* **7**: 619–630. doi: 10.1111/2041-210X.12528.

Bahat O. 1989. *Aspects in the ecology and biodynamics of the Golden Eagle (Aquila chrysaetos homeyeri) in the arid regions of Israel.* Master's thesis, Tel Aviv University.

Barnett AH, Moorcroft PR. 2008. Analytic steady-state space use patterns and rapid computations in mechanistic home range analysis. *Journal of Mathematical Biology* **57**: 139–159. doi: 10.1007/s00285-007-0149-8.

Bivand R, Lewin-Koh N. 2016. maptools: Tools for Reading and Handling Spatial Objects.
URL `https://cran.r-project.org/package=maptools`

Blackwell PG. 1997. Random diffusion models for animal movement. *Ecological Modelling* **100**: 87–102. doi: 10.1016/S0304-3800(97)00153-1.

Braham M, Miller T, Duerr AE, Lanzone M, Fesnock A, LaPre L, Driscoll D, Katzner T. 2015. Home in the heat: Dramatic seasonal variation in home range of desert golden

eagles informs management for renewable energy development. *Biological Conservation* **186**: 225–232. doi: 10.1016/j.biocon.2015.03.020.

Breed GA, Golson EA, Tinker MT. 2017. Predicting animal home-range structure and transitions using a multistate Ornstein-Uhlenbeck biased random walk. *Ecology* **98**: 32–47. doi: 10.1002/ecy.1615.

Burt WH. 1943. Territoriality and home range concepts as applied to mammals. *Journal of Mammalogy* **24**: 346–352. doi: 10.2307/1374834.

Collopy M, Edwards T. 1989. Territory Size, Activity Budget, and Role of Undulating Flight in Nesting Golden Eagles. *Journal of Field Ornithology* **60**: 43–51.

Collopy MW. 1984. Parental care and feeding ecology of golden eagle nestlings. *The Auk* **101**: 753–760.

Duerr AE, Miller TA, Lanzone M, Brandes D, Cooper J, O'Malley K, Maisonneuve C, Tremblay J, Katzner T. 2012. Testing an emerging paradigm in migration ecology shows surprising differences in efficiency between flight modes. *PLoS ONE* **7**: e35548. doi: 10.1371/journal.pone.0035548.

Dunn JE, Gipson PS. 1977. Analysis of radio telemetry data in studies of home range. *Biometrics* **33**: 85–101.

Eisaguirre JM, Booms TL, Barger CP, Lewis SB, Breed GA. 2019. Step selection functions on energy landscapes reveal how linear features alter migration movement in a large soaring bird. *bioRxiv* doi: 10.1101/805374.

Forester JD, Im HK, Rathouz PJ. 2009. Accounting for animal movement in estimation of resource selection functions: sampling and data analysis. *Ecology* **90**: 3554–3565.

Fortin D, Beyer HL, Boyce MS, Smith DW, Duchesne T, Mao JS. 2005. Wolves influence elk movements: behavior shapes a trophic cascade in Yellowstone National Park. *Ecology* **86**: 1320–1330. doi: 10.1890/04-0953.

Getty T. 1981. Analysis of central-place space-use patterns: the elastic disc revisited. *Ecology* **62**: 907–914. doi: 10.2307/1936988.

Gill FB. 2007. *Ornithology.* New York: W. H. Freeman and Company, third edition.

Herzog J, Eisaguirre JM, Linkhart B, Booms TL. 2019. Golden eagle diet in western Alaska. *Journal of Raptor Research* **53**: 393–401. doi: 10.3356/0892-1016-53.4.393.

Hollister J, Shah T. 2018. elevatr: access elevation data from various APIs. URL https://cran.r-project.org/package=elevatr

Hooten MB, Hanks EM, Johnson DS, Alldredge MW. 2014. Temporal variation and scale in movement-based resource selection functions. *Statistical Methodology* **17**: 82–98. doi: 10.1016/j.stamet.2012.12.001.

Hooten MB, Johnson DS, McClintock BT, Morales JM. 2017. *Animal movement: statistical models for telemetry data.* New York: CRC Press.

Huxley J. 1934. A natural experiment on territorial instinct. *British Birds* **27**: 270–277.

Johnson DS, Hooten MB, Kuhn CE. 2013. Estimating animal resource selection from telemetry data using point process models. *Journal of Animal Ecology* **82**: 1155–1164. doi: 10.1111/1365-2656.12087.

Johnson DS, Thomas DL, Ver Hoef JM, Christ A, Service F. 2008. A general framework for the analysis of animal resource selection from telemetry data. *Biometrics* **64**: 968–976. doi: 10.1111/j.1541-0420.2007.00943.x.

Katzner TE, Brandes D, Miller T, Lanzone M, Maisonneuve C, Tremblay JA, Mulvihill R, Merovich GT. 2012. Topography drives migratory flight altitude of golden eagles: implications for on-shore wind energy development. *Journal of Applied Ecology* **49**: 1178–1186. doi: 10.1111/j.1365-2664.2012.02185.x.

Katzner TE, Turk PJ, Duerr AE, Miller TA, Lanzone MJ, Cooper JL, Brandes D, Tremblay JA, Lemaître J. 2015. Use of multiple modes of flight subsidy by a soaring ter-

507 restrial bird, the golden eagle Aquila chrysaetos, when on migration. *Journal of Royal*
508 *Society Interface* **12**: 20150530. doi: 10.1098/rsif.2015.0530.

509 Kochert MN, Steenhof K, McIntyre CL, Craig EH. 2002. Golden Eagle (Aquila chrysae-
510 tos). In Poole A (ed.) *The Birds of North America*. Ithaca: Cornell Lab of Ornithology.

511 Lele S, Keim J. 2006. Weighted distributions and estimation of resource selection prob-
512 ability functions. *Ecology* **87**: 3021–3028. doi: 10.12968/ajmw.2019.0008.

513 Lish JW, Domenech R, Bedrosian BE, Ellis DH, Payton M. 2016. Wing Loading in North
514 American Golden Eagles (Aquila chrysaetos). *Journal of Raptor Research* **50**: 70–75.
515 doi: 10.3356/rapt-50-01-70-75.1.

516 Macander MJ, Swingley CS, Joly K, Raynolds MK. 2015. Landsat-based snow persis-
517 tence map for northwest Alaska. *Remote Sensing of Environment* **163**: 23–31. doi:
518 10.1016/j.rse.2015.02.028.

519 Manly BFJ, Lyman L, Thomas D, McDonald TL, Erickson W. 2002. *Resource selection by*
520 *animals: statistical design and analysis for field studies*. Dordrecht: Kluwer Academic
521 Publishers.

522 McIntyre CL, Adams LG. 1999. Reproductive characteristics of migratory Golden Eagles
523 in Denali National Park, Alaska. *The Condor* **101**: 115–123. doi: 10.2307/1370452.

524 McIntyre CL, Schmidt JH. 2012. Ecological and environmental correlates of territory
525 occupancy and breeding performance of migratory Golden Eagles Aquila chrysaetos in
526 interior Alaska. *Ibis* **154**: 124–135. doi: 10.1111/j.1474-919X.2011.01181.x.

527 Michelot T, Langrock R, Patterson TA. 2016. moveHMM: an R package for the statistical
528 modelling of animal movement data using hidden Markov models. *Methods in Ecology*
529 *and Evolution* **7**: 1308–1315. doi: 10.1111/2041-210X.12578.

530 Moorcroft P, Lewis M. 2006. *Mechanistic home range analysis*. Princeton, NJ: Princeton
531 University Press.

532 Moorcroft PR, Barnett A. 2008. Mechanistic home range models and resource selection
533   analysis: a reconciliation and unification. *Ecology* **89**: 1112–1119. doi: 10.1890/06-
534   1985.1.

535 Morales JM, Ellner SP. 2002. Scaling up animal movements in heterogeneous land-
536   scapes: the importance of behavior. *Ecology* **83**: 2240–2247. doi: 10.1890/0012-
537   9658(2002)083[2240:SUAMIH]2.0.CO;2.

538 Moss EH, Hipkiss T, Ecke F, Dettki H, Sandström P, Bloom PH, Kidd JW, Thomas SE,
539   Hörnfeldt B. 2014. Home-range size and examples of post-nesting movements for adult
540   Golden Eagles (Aquila chrysaetos) in boreal Sweden. *Journal of Raptor Research* **48**:
541   93–105. doi: 10.3356/jrr-13-00044.1.

542 Murgatroyd M, Photopoulou T, Underhill LG, Bouten W, Amar A. 2018. Where eagles
543   soar: Fine-resolution tracking reveals the spatiotemporal use of differential soaring
544   modes in a large raptor. *Ecology and Evolution* **8**: 6788–6799. doi: 10.1002/ece3.4189.

545 Nathan R, Getz WM, Revilla E, Holyoak M, Kadmon R, Saltz D, Smouse PE. 2008. A
546   movement ecology paradigm for unifying organismal movement research. *Proceedings*
547   *of the National Academy of Sciences* **105**: 19052–9. doi: 10.1073/pnas.0800375105.

548 Potts JR, Bastille-Rousseau G, Murray DL, Schaefer JA, Lewis MA. 2014a. Predicting
549   local and non-local effects of resources on animal space use using a mechanistic step
550   selection model. *Methods in Ecology and Evolution* **5**: 253–262. doi: 10.1111/2041-
551   210X.12150.

552 Potts JR, Harris S, Giuggioli L. 2012. Territorial dynamics and stable home range for-
553   mation for central place foragers. *PLoS ONE* **7**. doi: 10.1371/journal.pone.0034033.

554 Potts JR, Lewis MA. 2014. How do animal territories form and change? Lessons from
555   20 years of mechanistic modelling. *Proceedings of the Royal Society B* **281**: 20140231.
556   doi: 10.1098/rspb.2014.0231.

Potts JR, Mokross K, Lewis MA. 2014b. A unifying framework for quantifying the nature of animal interactions. *Journal of The Royal Society Interface* **11**: 20140333. doi: 10.1098/rsif.2014.0333.

Potts JR, Mokross K, Stouffer PC, Lewis MA. 2014c. Step selection techniques uncover the environmental predictors of space use patterns in flocks of Amazonian birds. *Ecology and Evolution* **4**: 4578–4588. doi: 10.1002/ece3.1306.

Prokopenko CM, Boyce MS, Avgar T. 2016. Characterizing wildlife behavioural responses to roads using integrated step selection analysis. *Journal of Applied Ecology* doi: 10.1111/1365-2664.12768.

R Core Team. 2018. R: a language and environment for statistical computing. URL https://www.r-project.org/

Schlather M, Malinowski A, Oesting M, Boecker D, Strokorb K, Engelke S, Martini J, Ballani F, Moreva O. 2019. Simulation and analysis of random fields. URL http://ms.math.uni-mannheim.de/de/publications/software/randomfields

Schooley RL, Wiens JA. 2004. Movements of cactus bugs: patch transfers, matrix resistance, and edge permeability. *Landscape Ecology* **19**: 801–810. doi: 10.1007/s10980-005-0093-2.

Shepard ELC, Wilson RP, Rees WG, Grundy E, Lambertucci SA, Vosper SB. 2013. Energy landscapes shape animal movement ecology. *The American Naturalist* **182**: 298–312. doi: 10.1086/671257.

Signer J, Fieberg J, Avgar T. 2019. Animal movement tools (amt): R package for managing tracking data and conducting habitat selection analyses. *Ecology and Evolution* **9**: 880–890. doi: 10.1002/ece3.4823.

Stan Development Team. 2016. rstanarm: Bayesian applied regression modeling via Stan. R package version 2.13.1.

583 Stan Development Team. 2018. RStan: the R interface to Stan, Version 2.17.3.

584 URL http://mc-stan.org

585 Watson J. 2010. *The Golden Eagle*. New Haven: Yale University Press, second edition.

586 Watson JW, Duff AA, Davies RW. 2014. Home range and resource selection by GPS-
587 monitored adult Golden Eagles in the Columbia Plateau Ecoregion: Implications for
588 wind power development. *Journal of Wildlife Management* **78**: 1012–1021. doi:
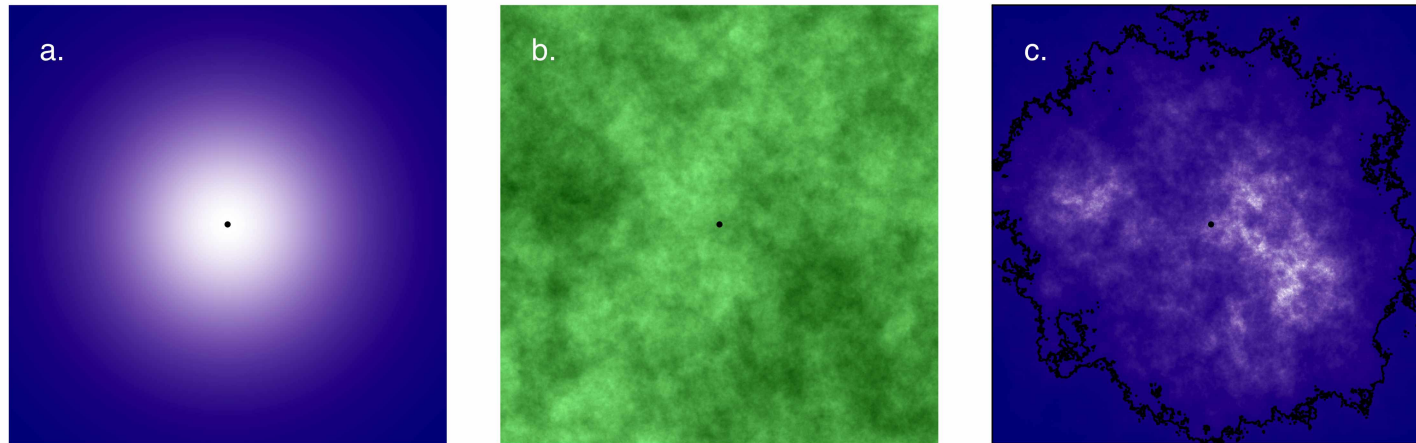589 10.1002/jwmg.745.

Figures

Figure 1: Example of computing the steady-state, analytical home range and space use distribution from an Ornstein-Uhlenbeck space use model. The movement-only, habitat-independent space use distribution (a) is modified by the habitat (b) and the animal's preferences for that habitat (i.e. a habitat weighting function), giving rise to a predicted space use distribution (c). Point is animal's center of attraction, and the polygon in c is the 95% volume contour of the space use distribution, representing an estimated home range boundary.
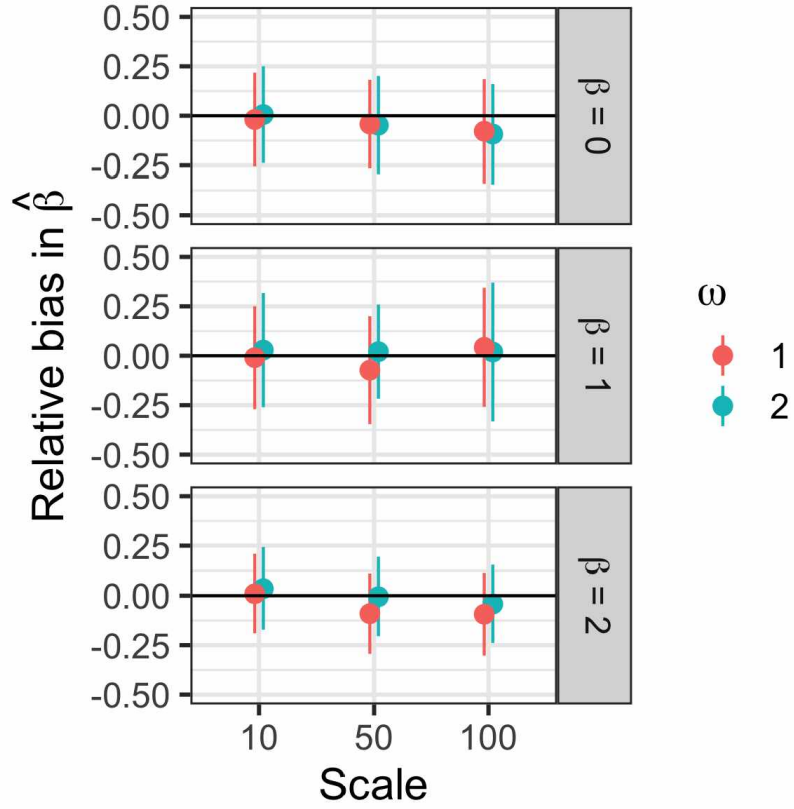
Figure 2: Summary of the relative bias in the selection coefficient β when estimated with an Ornstein-Uhlenbeck home range model with movement parameters estimated offline. The 'scale' parameter adjusts the level of spatial autocorrelation over the artificial landscape movements were simulated on, and ω is a movement parameter. Points are the average of posterior means computed across 100 simulations $\pm$ two standard deviations.
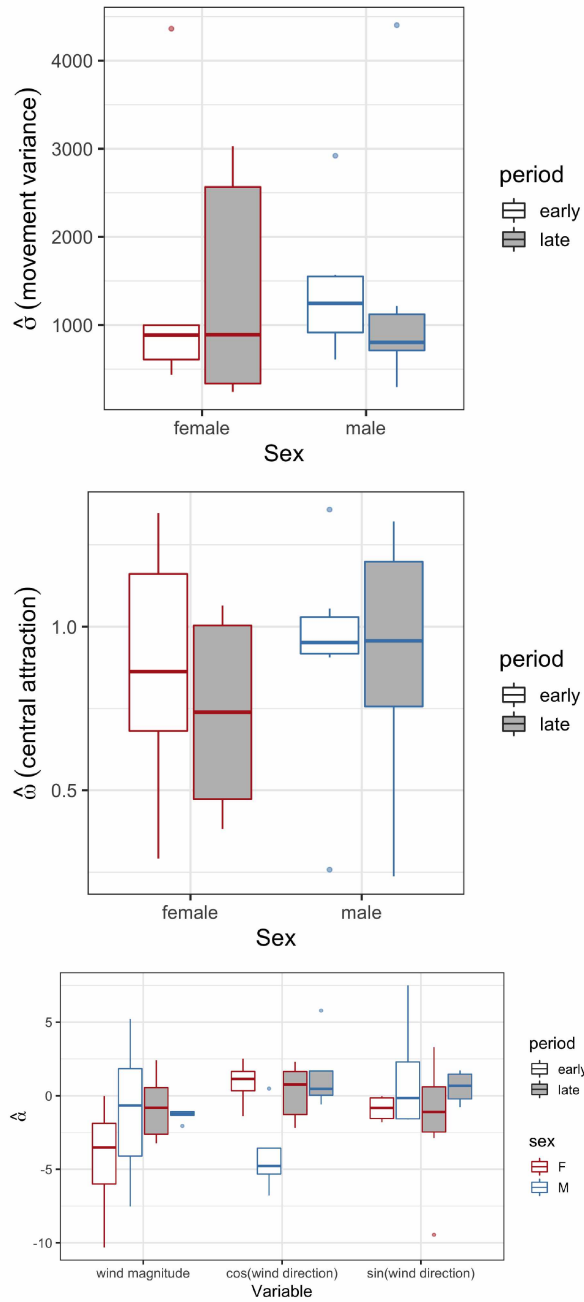
Figure 3: Summary of the posterier means of the movement parameters in an Ornstein-Uhlenbeck movement model fit to six male and six female golden eagles with territories in southcentral Alaska. σ is the movement variance; ω the autocorrelation parameter measuring the centralizing tendency; and $\boldsymbol{\alpha}$ the coefficients in the Markovian home range core switching process. The models were fit separately for early and late breeding season.
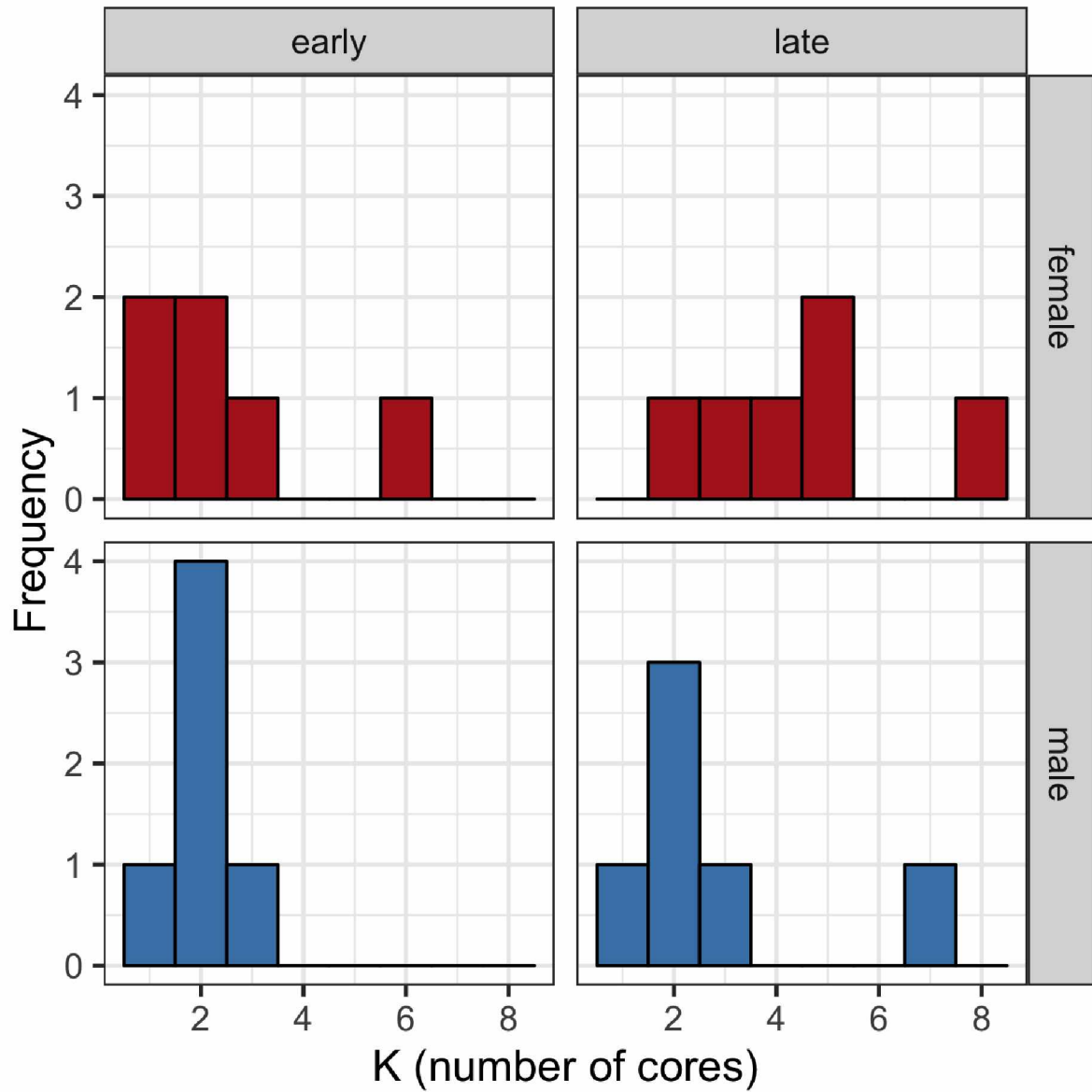
Figure 4: Number of home range cores estimated with a k-means clustering algorithm for six male and six female golden eagles with territories in southcentral Alaska. The algortithm was run separately for early and late breeding season.
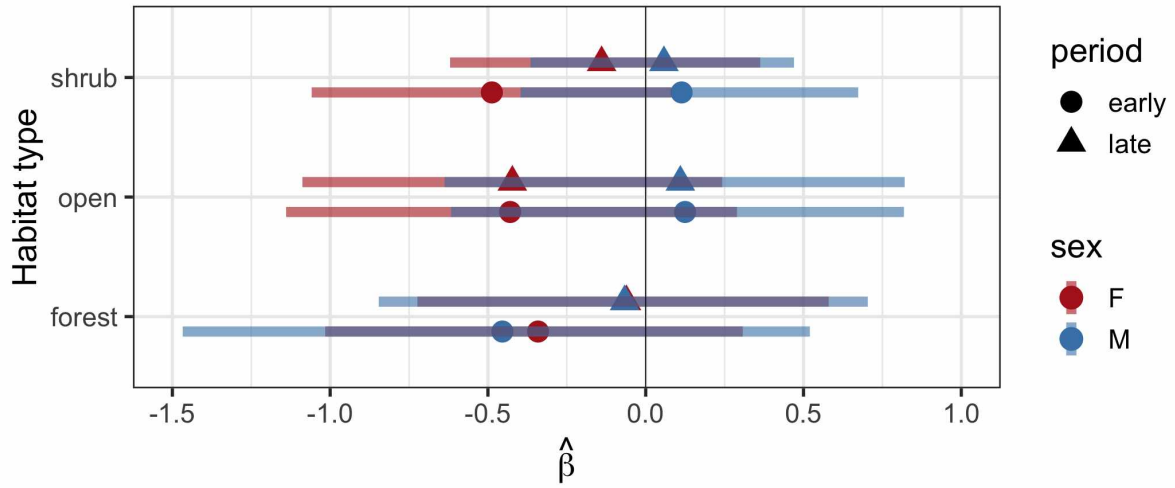
Figure 5: Population-level estimates of the habitat selection parameters estimated with an Ornstein-Uhlenbeck space use model for territorial golden eagles summering in south-central Alaska. Points are posterior means and horizontal lines are 95% credible intervals. The reference category used for estimation was 'bare'.
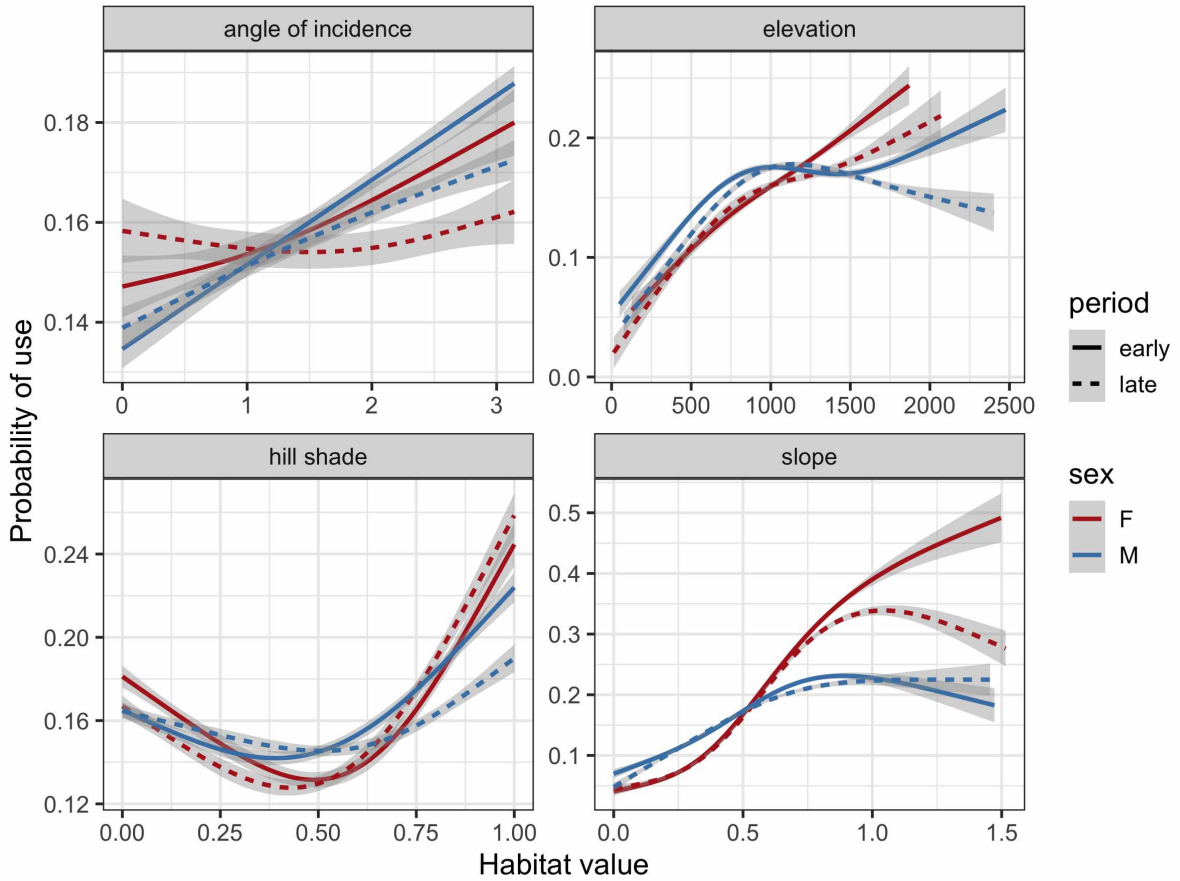
Figure 6: Probability of a golden eagle using a spatial location within its breeding season home range in southcentral Alaska as a function of habitat variables estimated with an Ornstein-Uhlenbeck (OU) space use model. This is the average effect conditioned on the space available to each eagle characterized by an OU biased random walk. The model was fit separately for early and late breeding season and for each sex. Predictions were smoothed over the availability points with a generalized additive model ($df = 4$) and ribbons are 95% confidence intervals. Units are radians for angle of incidence and slope, and meters for elevation. Higher hill shade corresponds to more direct sun and greater thermal uplift potential.
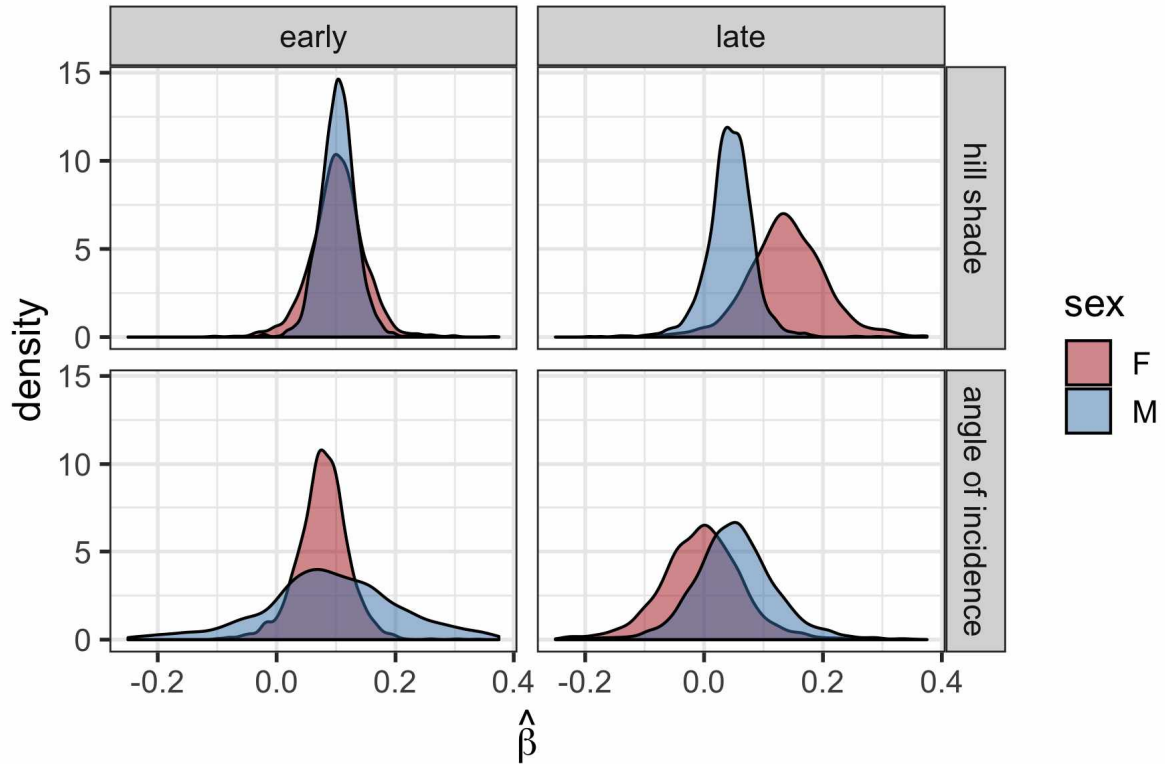
Figure 7: Marginal posterior densities of population-level estimates of the hill shade and angle of incidence parameters showing partitioning of the energy landscape (thermal and orographic uplift) by male and female golden eagles during late breeding season. These were estimated with an Ornstein-Uhlenbeck space use model for territorial golden eagles summering in southcentral Alaska. Densities were constructed with 2000 posterior samples.
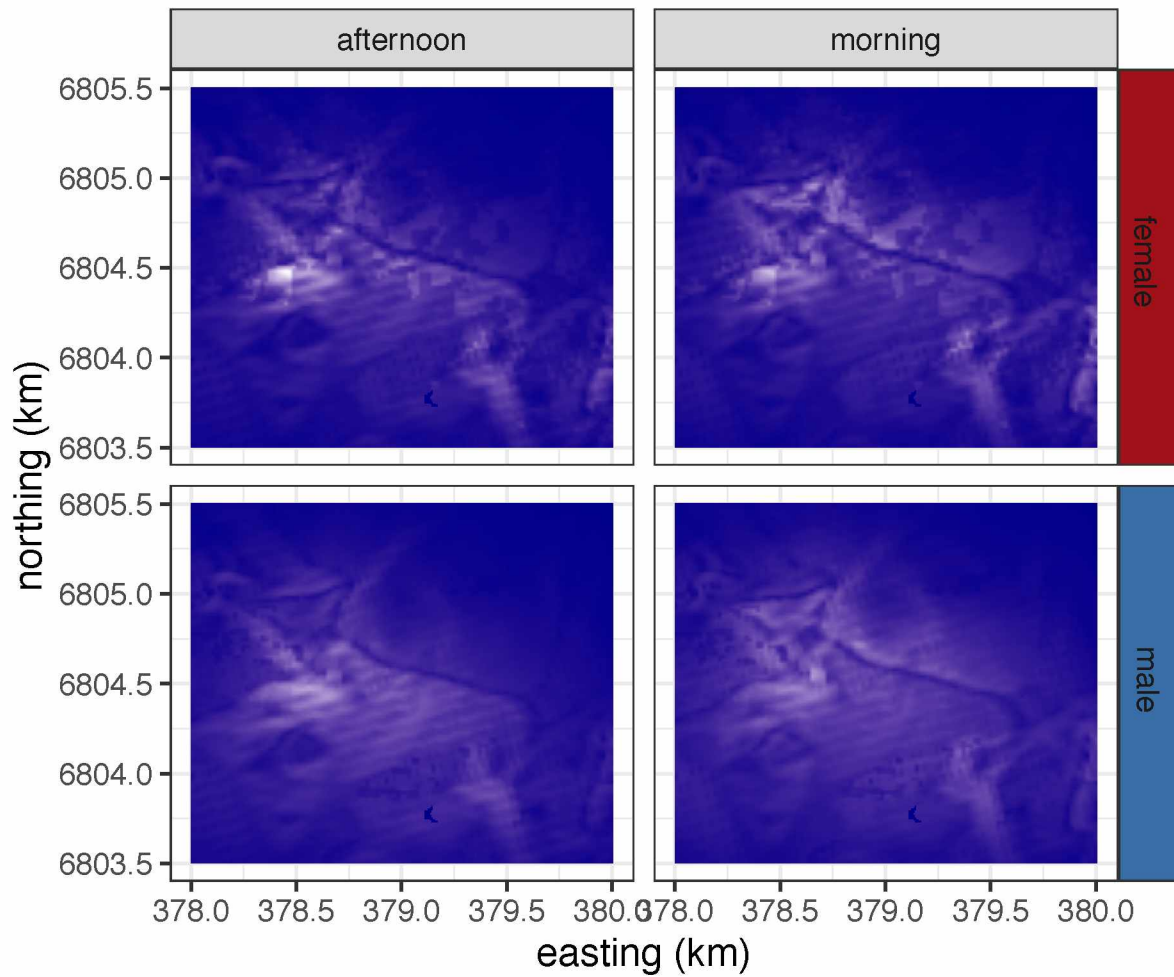
Figure 8: Space use distributions predicted from the Ornstein-Uhlenbeck space use model for territorial golden eagles summering in southcentral Alaska. Predictions were made over a characteristic landscape for morning and afternoon to illustrate differential use patterns according to thermal uplift. White corresponds to higher probability of use and blue lower.
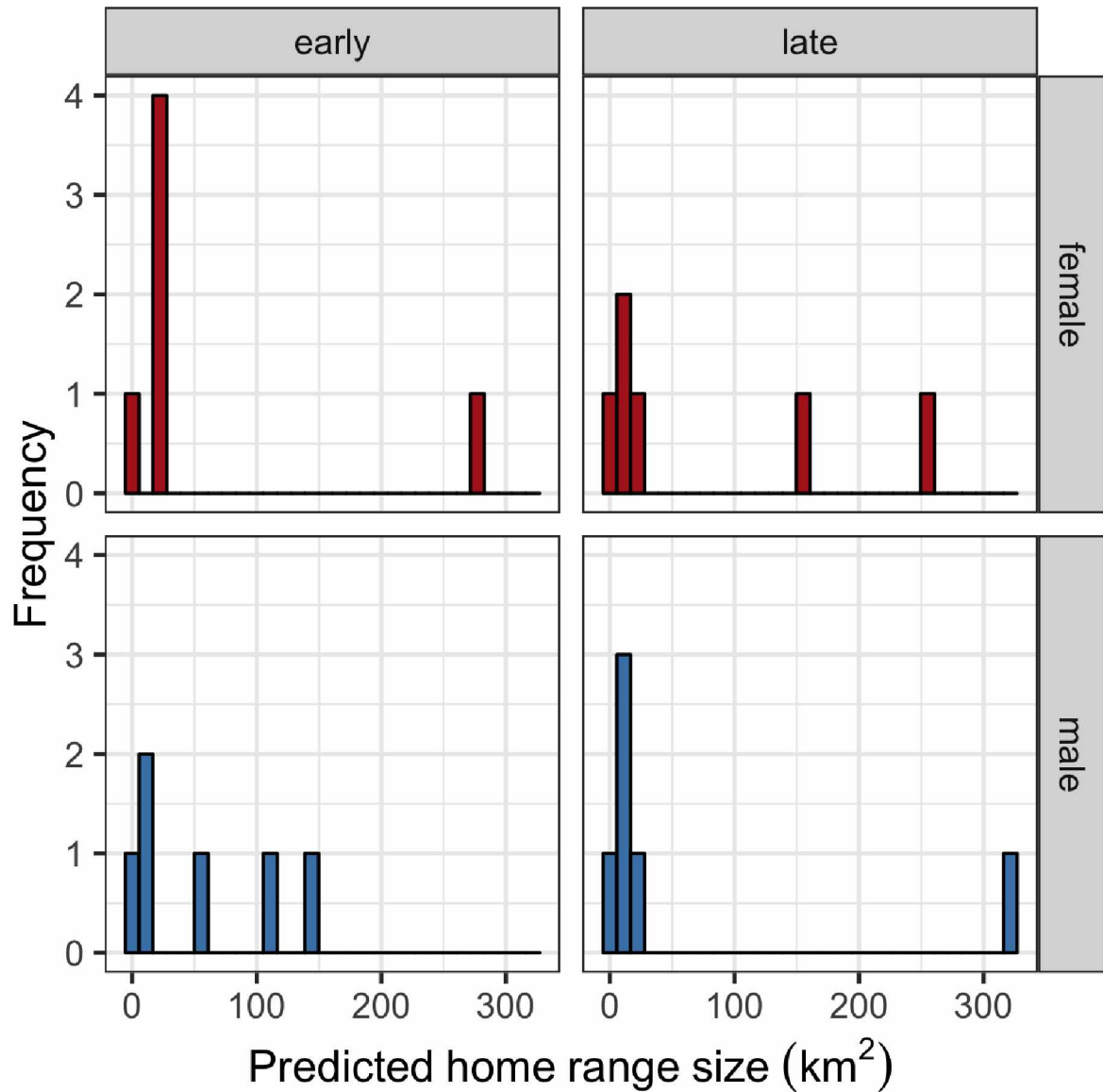
Figure 9: Home range sizes predicted from the Ornstein-Uhlenbeck space use model for territorial golden eagles summering in southcentral Alaska. Home range size was estimated as the 95% volume contour of the predicted space use distribution.
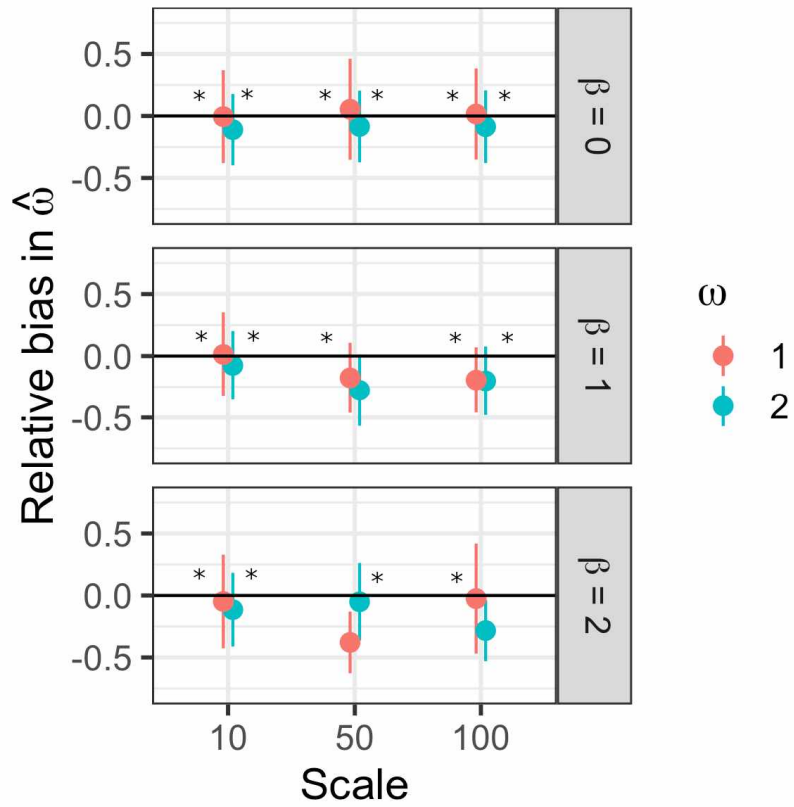
Appendix 1: supplementary tables and figures

Figure S1: Relative bias in centralizing tendency when estimated with Ornstein-Uhlenbeck home range model with movement parameters estimated offline. Asterisk indicates 95% credible set captured the true value in $> 70\%$ of the simulations.
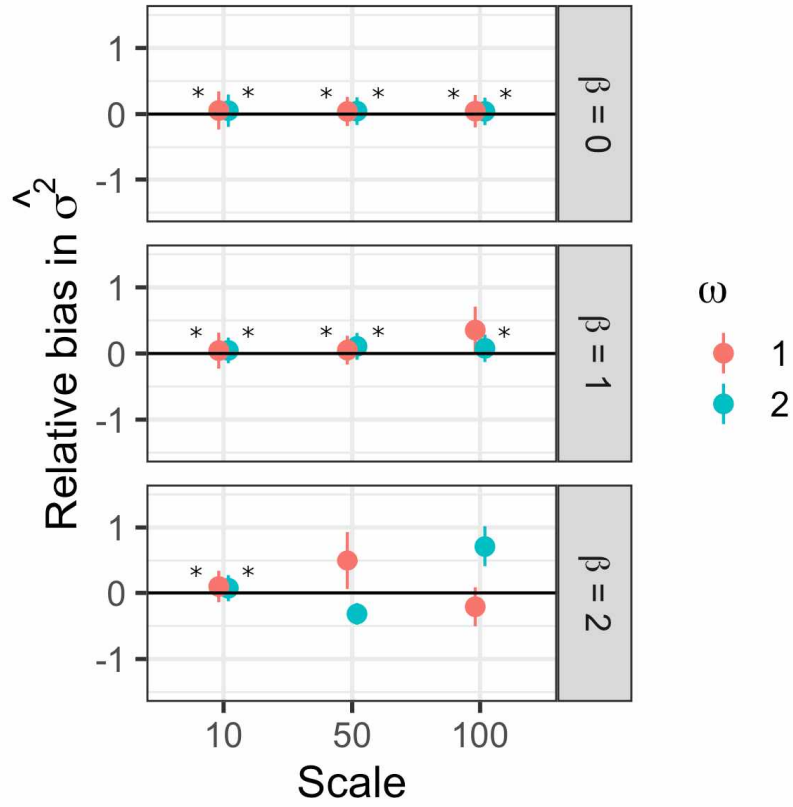
Figure S2: Relative bias in centralizing tendency when estimated with Ornstein-Uhlenbeck home range model with movement parameters estimated offline. Asterisk indicates 95% credible set captured the true value in > 70% of the simulations.

Table S1: Habitat types used in analysis.

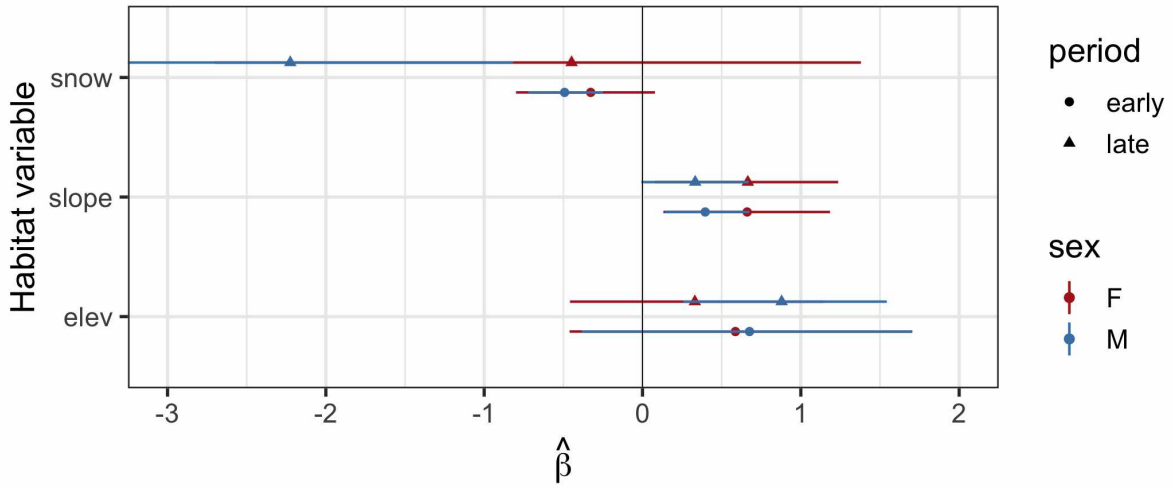| AKVWC class	habitat type
'Bareground'	'bare'
'Freshwater or Saltwater'	'water'
'Bareground (Beach or Tide Flat) (Southern Alaska)', 'Herbaceous (Marsh) (Interior Alaska, Cook Inlet Basin)', 'Herbaceous (Marsh) (Northern and Western Alaska)', 'Herbaceous (Tidal) (Southern Alaska)', 'Herbaceous (Wet-Marsh) (Southern Alaska)', 'Herbaceous (Aquatic)', 'Low Shrub (Tidal) (Southern Alaska)', 'Herbaceous (Wet-Marsh) (Tidal)'	'wet'
'Herbaceous (Mesic) (Interior Alaska, Cook Inlet Basin)', 'Herbaceous (Mesic) (Northern and Western Alaska)', 'Herbaceous (Mesic) (Southern Alaska)', 'Herbaceous (Peatland) (Southern Alaska)', 'Herbaceous (Wet) (Interior Alaska, Cook Inlet Basin)', 'Herbaceous (Wet) (Northern and Western Alaska)', 'Lichen', 'Moss', 'Moss (Southern Alaska)', 'Sparse Vegetation (Interior Alaska, Cook Inlet Basin)', 'Sparse Vegetation (Northern and Western Alaska)', 'Tussock Tundra (Low shrub or Herbaceous)', 'Fire Scar'	'open'
'Low Shrub', 'Low Shrub (Peatland) (Southern Alaska)', 'Dwarf Shrub', 'Dwarf Shrub (Southern Alaska)', 'Dwarf Shrub-Lichen', 'Dwarf Shrub, or Herbaceous (Mesic) (Southern Alaska)', 'Low Shrub or Tall Shrub (Open-Closed)', 'Low Shrub/Lichen', 'Low-Tall Shrub (Southern Alaska)', 'Tall Shrub (Open-Closed)'	'shrub'
'Deciduous Forest (Open-Closed)', 'Deciduous Forest (Open-Closed) (Seasonally Flooded) (Southern Alaska)', 'Deciduous Forest (Woodland-Closed) (Southern Alaska)', 'Hemlock (Woodland-Closed)', 'Hemlock-Sitka Spruce (Woodland-Closed)', 'Needleleaf Forest (Open-Closed) (Seasonally Flooded) (Southern Alaska)', 'Needleleaf Forest (Woodland-Open) (Peatland) (Southern Alaska)', 'Sitka Spruce (Woodland-Closed)', 'White Spruce or Black Spruce (Open-Closed)', 'White Spruce or Black Spruce (Woodland)', 'White Spruce or Black Spruce-Deciduous (Open-Closed)', 'White Spruce or Black Spruce/Lichen (Woodland-Open)'	'forest'
'Urban, Agriculture, Road'	'human'
'Ice-Snow'	'ice'

Figure S3: Population-level estimates of the habitat selection parameters estimated with an Ornstein-Uhlenbeck space use model for territorial golden eagles summering in south-central Alaska. The snow variable was a dynamic indicator of whether or not a location was snow-free. Points are posterior means and horizontal lines are 95% credible intervals.
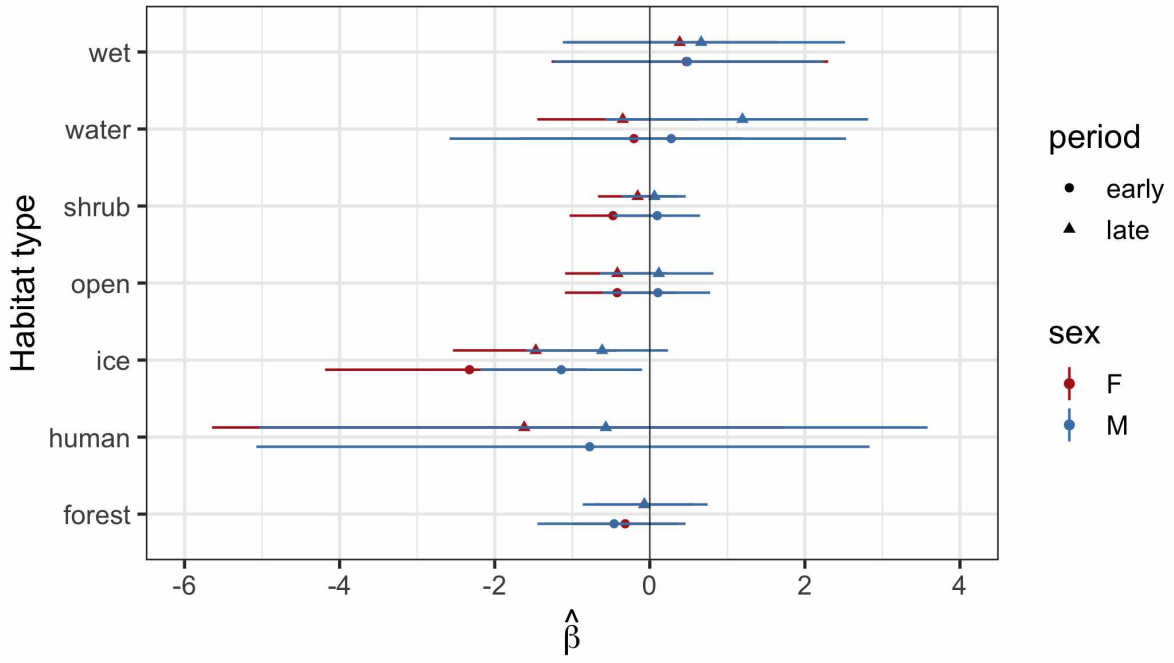
Figure S4: Full version of figure 5 from main text.

Appendix 2: code

Stan model

```
data {

    int<lower=0> N;              // length of track

    vector[N] dt;                // time intervals

    vector[2] x[N];              // observed locations

    int<lower=1> K;              // number of states

    vector[2] mu[K];             // central points

    int mumu[N];                 // 'known' state sequence

    vector[K] wm[N];             // wind magnitude for each core

    vector[K] wc[N];             // cosine wind direction at each core

    vector[K] ws[N];             // sine wind direction at each core

    matrix[K,K] d_mu;            // inter core distance matrix

}


parameters {

    real<lower=0> omega[K];      // attraction strength

    real<lower=0> sigma[K];      // diffusion parameter

    matrix[K,K] b;               // intercepts

    matrix[K,K] b_wm;            // coefficient for wind magnitude

    matrix[K,K] b_d;             // coefficient for inter-core distance

    matrix[K,K] b_wc;            // coefficient for cos(wind direction)

    matrix[K,K] b_ws;            // coefficient for sin(wind direction)

}

```

41

```
620

621

622  model {

623

624     matrix[2,2] Sigma; // var-cov matrix

625     matrix[2,2] Omega; // central attraction matrix

626

627     for (n in 2:N) {

628

629        // state is categorical draw

630        mumu[n] ~ categorical_logit( b[,mumu[n-1]] + b_d[,mumu[n-1]].*d_mu[,mumu[n-1]]

631     + b_wm[,mumu[n-1]].*wm[n-1] + b_wc[,mumu[n-1]].*wc[n-1]

632     + b_ws[,mumu[n-1]].*ws[n-1]);

633

634        //  define movement param matrices

635        Sigma[1,1] = sigma[mumu[n]];

636        Sigma[1,2] = 0;

637        Sigma[2,1] = 0;

638        Sigma[2,2] = sigma[mumu[n]];

639

640        Omega[1,1] = -omega[mumu[n]];

641        Omega[1,2] = 0;

642        Omega[2,1] = 0;

643        Omega[2,2] = -omega[mumu[n]];

644

645        // movement equation

646        x[n] ~ multi_normal(mu[mumu[n]] + matrix_exp(Omega*dt[n])

647     * ( x[n-1] - mu[mumu[n]] ),

648  Sigma - matrix_exp(Omega*dt[n]) * Sigma * matrix_exp(Omega'*dt[n]) );
```

```stan
649
650     }

651

652

653     // some priors
654     sigma ~ normal(6000000, 1000000);
655     omega ~ normal(0, 1);
656     to_vector(b_wm) ~ normal(0, 10);
657     to_vector(b_ws) ~ normal(0, 10);
658     to_vector(b_wc) ~ normal(0, 10);
659     to_vector(b_d) ~ normal(0, 10);
660     to_vector(b) ~ normal(0, 10);

661

662 }

663

664

665 generated quantities{

666

667

668     matrix[2,2] Sigma;
669     matrix[2,2] Omega;
670     vector[2] x_av[N];

671

672

673     for(i in 2:N){

674

675       Sigma[1,1] = sigma[mumu[i]];
676       Sigma[1,2] = 0;
677       Sigma[2,1] = 0;
```

```
678    Sigma[2,2] = sigma[mumu[i]];

679

680    Omega[1,1] = -omega[mumu[i]];

681    Omega[1,2] = 0;

682    Omega[2,1] = 0;

683    Omega[2,2] = -omega[mumu[i]];

684

685

686     x_av[1] = x[1];  // start somewhere

687

688     // this draws available points from posterior predictive

689     x_av[i] = multi_normal_rng(mu[mumu[i]] + matrix_exp(Omega*dt[i])

690   * ( x[i-1] - mu[mumu[i]] ),

691   Sigma - matrix_exp(Omega*dt[i]) * Sigma * matrix_exp(Omega'*dt[i]) );

692

693    }

694

695

696

697

698  }
```

R code

```
701   ##########################################
702   ### This chunk is done per individual###
703   ##########################################
704
705   ### samples from posterior of multistate OU model
```

```
706  stan.fit = stan("stan_model.stan",
707                    data = list(x,dt,N,K,mu,mumu,wm,ws,wc,d_mu),
708                    pars=c('omega', 'sigma','b','b_d','b_wm','b_wc','b_ws','x_av'),
709                    chains = 3,
710                    iter = 3000,
711                    warmup = 2000,
712                    cores = 3,
713                    control = list(max_treedepth = 13),
714                    seed = 3)  ### retains 3000 samples for inference
715
716
717  ### draws available points from posterior predictive
718  n_av = 5  # 5 available points per used poinst
719
720  x.av=matrix(rep(0,n_av), nrow = 1)
721  y.av=matrix(rep(0,n_av), nrow = 1)
722
723  for(k in 1:N){
724    x.av = rbind(x.av,sample(unlist(rstan::extract(stan.fit,
725                                    pars = paste0('x_av[',k,',1]')),
726                        use.names=F), n_av))
727    y.av = rbind(y.av,sample(unlist(rstan::extract(stan.fit,
728                                    pars = paste0('x_av[',k,',2]')),
729                        use.names=F), n_av))
730  }
731
732  x.av = x.av[-1,]
733  y.av = y.av[-1,]
734
```

```
735

736

737

738    ####################################################
739    ### This chunk estimates RSF across individuals ###
740    ####################################################
741
742    # use = bernouli used/available
743    # snow = binary indicator
744    # hab = categogrical habitat types
745    # elev_s = centered and standardized elevation
746    # slope_s = centered and standardized slope
747    # aoi_s = centered and standardized angle of incidence
748    # hs_s = centered and standardized hill shade
749    # mumu = home range core
750    # id = individual id
751    # rsf_dat = data frame holding above variables
752
753    rsf_bfit = stan_glmer(use ~ id   # fixed effect of id to account f
754                                     # or variation in availability among individuals
755                    + snow + (0+snow||id/mumu)
756                    + hab + (0+hab||id/mumu)
757                    + elev_s + (0+elev_s||id/mumu)
758                    + slope_s + (0+slope_s||id/mumu)
759                    + aoi_s + (0+aoi_s||id/mumu)
760                    + hs_s + (0+hs_s||id/mumu)
761                    + offset(aniso),
762                    family=binomial(link='logit'),
763                    data = rsf_dat,
```

```
cores = 4,

iter = 2500,

warmup = 1500,

thin = 2,

algorithm = 'sampling',

init_r = 0.5,  ## this helps chains initialize

adapt_delta = 0.95)
```